



This is the accepted manuscript made available via CHORUS. The article has been published as:

Incomplete mixing and reactions in laminar shear flow

A. Paster, T. Aquino, and D. Bolster

Phys. Rev. E **92**, 012922 — Published 31 July 2015

DOI: [10.1103/PhysRevE.92.012922](https://doi.org/10.1103/PhysRevE.92.012922)

Incomplete mixing and reactions in laminar shear flow

A. Paster*

*School of Mechanical Engineering, Faculty of Engineering,
Tel Aviv University, Tel Aviv 69978, Israel*

T. Aquino[†] and D. Bolster[‡]

*Dept. of Civil and Environmental Engineering and Earth Sciences,
University of Notre Dame, Notre Dame, IN 46556, USA*

(Dated: June 25, 2015)

Abstract

Incomplete mixing of reactive solutes is well known to slow down reaction rates relative to what would be expected from assuming perfect mixing. In purely diffusive systems, for example, it is known that small initial fluctuations in reactant concentrations can lead to reactant segregation, which in the long run can reduce global reaction rates due to poor mixing. In contrast, non-uniform flows can enhance mixing between interacting solutes. Thus a natural question arises: Can non-uniform flows sufficiently enhance mixing to restrain incomplete mixing effects, and if so, under what conditions? We address this question by considering a specific and simple case, namely a laminar pure shear reactive flow. Two solution approaches are developed: a novel Lagrangian random walk method and a semi-analytical solution. The results consistently highlight that if shear effects in the system are not sufficiently strong, incomplete mixing effects initially similar to purely diffusive systems will occur, slowing down the overall reaction rate. Then, at some later time, dependent on the strength of the shear, the system will return to behaving as if it were well-mixed, but represented by a reduced effective reaction rate.

PACS numbers: 05.10.Gg, 05.10.Ln, 47.70.Fw, 82.40.Ck

* paster@tau.ac.il

† tdecampo@nd.edu

‡ dbolster@nd.edu

I. INTRODUCTION

Chemical reactions driven by mixing are important processes that occur in a wide variety of engineered and natural flows. Some common examples of practical interest include atmospheric flows [1], oceanographic flows [2], riverine flows [3], limnologic flows [4] and industrial reactors [5] to mention but a few. One of the perhaps most obvious but critical features to recognize in any reactive system is that in order for reactions to actually occur the chemicals involved in the reaction must physically come into contact with one another. Mixing is the physical process that enables this contact to occur. In flowing systems this is inherently a fluid dynamics problem as flows can act in such a way as to enhance, or indeed suppress, mixing and thus chemical reactions.

While it is broadly recognized that non-uniform flows can enhance mixing, there is increasing evidence that current models do not adequately characterize these mixing processes, often overestimating reaction rates relative to what is observed in field and laboratory experiments [6–13]. This is likely due to the fundamental difference between the enhanced spreading/stretching of solutes that non-uniform flows induce, as quantified for example by an effective dispersion coefficient, and the true degree of mixing that actually occurs [14]. While spreading and mixing are intricately related and indeed historically the words have been used interchangeably, it is important to highlight that they are different processes. This is because spreading may not account for subscale fluctuations in concentrations that are critical to understanding mixing. Thus, there is a need for improved models that can accurately capture the nature of reactive transport. In this work we argue that Lagrangian-based approaches are naturally conducive to capturing these effects. To understand this issue in greater detail we focus on the irreversible bimolecular reaction $A + B \rightarrow P$, which can be regarded as the fundamental building block of more complex reaction chains (see ref. 15 for a detailed discussion).

A rich body of literature exists exploring the effects of incomplete mixing on reactions in purely diffusive systems [16–21]. Consider the following classical experiment where a domain is initially filled with equal total amounts of A and B , such that $C_A(x, t = 0) = C_B(x, t = 0) = C_0$, where A and B move by diffusion and react with one another kinetically with some known rate coefficient k . For this setup there is an analytical solution $C_A(x, t) = C_B(x, t) = C_0/(1 + kC_0t)$, which at late times scales like inverse time, or t^{-1} . It is important to note

that this analytical solution relies implicitly on the assumption that the concentrations are completely uniform and equal in space, or in other words that they are always well-mixed. If however, there is some stochastic fluctuation of the concentration fields around their mean value, this late time scaling will break down. For such systems, it has been shown that the late time mean concentration of the species will scale as $t^{-d/4}$ where d is the number of spatial dimensions in the system under consideration[18, 21]. Stochastic fluctuations are ubiquitous in real systems and so such breakdowns should perhaps be regarded as the norm rather than the exception.

Specifically, for such systems, at early times, fluctuations about the mean concentration are often small enough to be discarded and the system behaves as if it were indeed well-mixed. However, due to the fact that reactions consume mass, as the mean concentrations become smaller, the relative influence of the fluctuations becomes increasingly important. Indeed, at late times isolated pockets, or so-called segregated *islands*, of each reactive constituent emerge and the reaction is limited by how quickly reactants can diffuse across the interfaces of these islands, resulting in the slower $t^{-d/4}$ scaling [16–18, 21]. This phenomenon often goes by the name of Ovchinnikov-Zeldovich segregation and this behaviour has been observed experimentally [19, 20].

This problem has also received a great deal of attention in systems where transport is not by local Fickian diffusion, but rather by anomalous dispersive transport, including nonlocal in space superdiffusive systems and nonlocal in time subdiffusive systems [22–24]. Such nonlocal transport is common in a broad array of disciplines including transport in porous media [25–27], streams [28], groundwater systems [29, 30] and biological systems [31] to name a few. In all cases similar late-time scalings for the mean concentration that deviate from the well-mixed t^{-1} scaling have been predicted and observed. The specific late time scaling will depend on the nature of the transport and the dimensionality of the problem being considered. However, to our knowledge, this problem has received limited attention in the context where transport is by advection and diffusion in a non-uniform velocity field. As noted above, it is well known that non-uniform velocity fields can significantly affect the nature of mixing and thus can in principle strongly impact mixing-driven reactions.

While much focus has been given to mixing in turbulent flows, it is important to recognize that mixing in non-uniform laminar flows can also result in very interesting mixing dynamics [32–38]. In this work we propose to study this problem in one of the simplest forms of non-

uniform flow, namely a pure laminar shear flow. Pure shear flows have received a great deal of attention in a variety of applications due to both their simplicity and ability to provide invaluable physical insight. Okubo [39, 40] studied transport in pure shear flows to better understand solute dispersion in rivers, estuaries, lakes and oceans. Novikov [41] used it as a model to study turbulent dispersion in streams. Others [42–44] highlight it as an important case in understanding turbulent dispersion. More recently it was shown [45] that from purely a mixing perspective, as quantified by the scalar dissipation rate [46, 47] or dilution index [48], a pure shear flow is incredibly efficient at mixing. The term *hypermixing* was used, emphasizing that the predicted mixing is even faster than conventional super-diffusion. Ref. 49 extended this to more complex flows using the Okubo-Weiss metric to quantify enhancement of mixing due to more general locally non-uniform velocity fields.

The above discussion leads us to ask the following question: Is mixing in a laminar shear flow sufficient to overcome incomplete mixing effects on the evolution of mean concentration in a reactive system or will incomplete mixing effects still persist? The answer to this question is addressed in this paper with the first application to a non-uniform flow of a random walk particle tracking method designed for reactive transport. It was originally developed for purely diffusive transport [50] and we extend it further. The results of this paper provide a general understanding of the influence of shear flows on incomplete mixing, paving the road for more general non-uniform velocity fields.

The paper is structured as follows. In Section II we present the governing equations for flow, transport and reaction for the chosen setup in dimensional and non-dimensional form. In Section III we discuss the initial conditions, focusing on both deterministic and stochastic initial conditions, which are at the root of incomplete mixing. In Section IV we describe the Lagrangian random walk particle tracking method for reactive transport. In Section V we present and discuss results obtained with this method. In Section VI we propose a semi-analytical model to interpret observations from Section V. We conclude with a discussion in Section VII.

II. GOVERNING EQUATIONS

We consider a bimolecular reactive system that is embedded in a uniform shear flow. Transport of the species is driven by a constant diffusion coefficient and advection according

117 to the uniform shear flow. The two constituents in this system, A and B , react kinetically
 118 and irreversibly with one another, i.e. $A + B \rightarrow P$. At this point we are not interested in
 119 what happens to the product P , but rather on how A and B are consumed, so the fate of P
 120 is neglected in this work. The flow in the system is completely independent of the transport,
 121 i.e. the flow is not affected by the concentration of the constituents. For an infinite two-
 122 dimensional space, the governing equation for transport is the advection-dispersion-reaction
 123 equation (ADRE), given for each of the species $i = A, B$ by

$$\frac{\partial C_i}{\partial t} + \alpha y \frac{\partial C_i}{\partial x} = \nabla \cdot (D \nabla C_i) - r_i \quad (1)$$

124 where $C_i(\mathbf{x}, t)$ is the concentration [mol L^{-d}], α is the shear rate [T^{-1}], D is the dispersion
 125 coefficient [$\text{L}^2 \text{T}^{-1}$].

126 The sink term, in our case, is the local rate of reaction, and is identical for A and B since
 127 they are consumed with a 1:1 stoichiometry ratio, i.e.

$$r_A = r_B = r . \quad (2)$$

128 We assume the law of mass action prevails for our system, and write the reaction rate as

$$r(C_A, C_B) = k C_A C_B , \quad (3)$$

129 where k [$\text{L}^d \text{mol}^{-1} \text{T}^{-1}$] is the kinetic rate constant for a given reaction. Thus, eq. (1)
 130 represents a coupled set.

131 A. Non-dimensional equations

132 We consider the following dimensionless variables

$$C^* = C/C_0, \quad t^* = k C_0 t, \quad \alpha^* = \alpha/(k C_0), \quad x^* = x/l, \quad y^* = y/l, \quad (4)$$

133 where l is a characteristic length associated with the initial fluctuations in concentration
 134 (e.g. a correlation length). Using these non-dimensional variables, our governing equation
 135 for transport becomes

$$\frac{\partial C_i^*}{\partial t^*} + \alpha^* y^* \frac{\partial C_i^*}{\partial x^*} = \frac{1}{\text{Da}} \nabla^{*2} C_i^* - C_A^* C_B^*, \quad (5)$$

136 where $\text{Da} = \frac{k_0 l^2}{D}$ is the Damköhler number, which quantifies the relative importance of
 137 reaction to transport by diffusion. In other words, it quantifies how quickly reactions happen
 138 relative to how quickly diffusion can homogenize a patch of size l . α^* is a dimensionless shear
 139 rate that quantifies the relative importance of shear to reaction. For the sake of convenience,
 140 we drop the stars from here on, and all the variables presented are non-dimensional.

141 III. INITIAL CONDITIONS

142 The focus of this work is the emergence of incomplete mixing of reactants as the system
 143 evolves, which is known to arise due to stochastic fluctuations in the concentration field
 144 [e.g. 18, 21–23]. Thus we focus on the case of a stochastic initial condition, i.e. the initial
 145 concentration comprises a mean contribution plus a stochastic or noise term. In this case,
 146 the exact concentration at a point is unknown and statistical information is available instead.

147 Specifically, we assume that for each of the species A and B , the stochastic initial con-
 148 centration field is given by an average value plus a white noise contribution. Decomposing
 149 the concentration into mean and a perturbation, we write for $i = A, B$

$$C_i(\mathbf{x}, t) = \overline{C}_i(\mathbf{x}, t) + C'_i(\mathbf{x}, t) \quad (6)$$

150 where $\overline{C}(\mathbf{x}, t)$ is the ensemble mean over all possible realizations. The perturbation C'_i has
 151 zero mean. The initial condition for the mean is given in a general manner by

$$\begin{aligned} \overline{C}_A(\mathbf{x}, t=0) &= C_{A0}(\mathbf{x}), \\ \overline{C}_B(\mathbf{x}, t=0) &= C_{B0}(\mathbf{x}) \end{aligned} \quad (7)$$

152 Assuming that the initial fluctuation term is Gaussian (or that higher order moments
 153 are irrelevant), the initial condition for the perturbation concentration of species i and j is
 154 defined by the covariance structure

$$\overline{C'_i(\mathbf{x}_1, t=0)C'_j(\mathbf{x}_2, t=0)} = \mu_{ij}(\mathbf{x}_1)\delta(\mathbf{x}_1 - \mathbf{x}_2) \quad (8)$$

155 where μ_{ij} is the white noise amplitude and δ is Dirac's Delta function. The white noise or
 156 delta-correlated initial condition is tantamount to assuming a very short range correlation in
 157 the fluctuations. The delta correlation has been shown to be a good approximation of other
 158 short range correlation structures such as exponential or Gaussian [51, 52] and is invoked
 159 for mathematical convenience.

In this work we assume the system is ergodic and statistically (space-)stationary, so that the mean concentration and the correlations depend only on relative position. We also assume that the species have an identical statistical structure, so that the initial mean concentrations are equal, and are given (in non-dimensional form) by

$$\overline{C_A}(t=0) = \overline{C_B}(t=0) = 1. \quad (9)$$

Furthermore, we assume that the magnitudes of fluctuation variances are equal and constant in space,

$$\mu_{AA} = \mu_{BB} = \mu, \quad (10)$$

and assume the species concentration fluctuations are initially uncorrelated, i.e.

$$\mu_{AB} = 0. \quad (11)$$

We restrict ourselves to this specific setup for a few reasons. First, this simple case provides a great deal of physical insight into the problem at hand. Second, it is straightforward to implement this set of initial conditions in a particle tracking algorithm, although more complex structures can readily be included. Third, a semi-analytical approximate solution to this system, for arbitrary dimension ($d = 1, 2, 3$) when shear is absent ($\alpha = 0$), is available from previous work [51], and can be used for comparison with the new results. Additionally, this approximate solution can, at least qualitatively, be extended to the shear problem as will be discussed below.

IV. NUMERICAL PARTICLE TRACKING SIMULATIONS

In this section we describe a Monte-Carlo-based particle tracking approach to finding numerical solutions for the system and equations presented so far. The approach is a novel extension of previous works [51, 53] which were restricted to purely diffusive transport. Here we extend the methodology to the case of uniform shear flow, with the long term goal of ultimately utilizing it to account for more complex, general flows.

The fundamental principle behind any particle tracking numerical method is to represent the concentration field by a cloud of discrete particles, representing elementary masses of solute. Time is discretized into finite time steps (not necessarily equal), and the ADRE is applied using the concept of operator splitting: in every time step, we first annihilate

any particles that would react as determined by a physically based probabilistic set of laws, representing reaction in the system; second, we move all surviving particles in a manner that represents both advection and diffusion in the system following classic random walk principles. The annihilation of particles is determined according to a local reaction probability, which is made up of two components, one based on the probability that two particles can collocate, which depends entirely on transport mechanisms, and the second based on the probability that reaction occurs given that particles have collocated, determined entirely by the kinetics of the reaction. The details are described in the following. Note that in this section we focus on the evolution of the system within a single time step Δt . Hence, for simplicity, and without loss of generality, we use $t = 0$ to denote the beginning of the time step.

A. Advection and diffusion

For the case of a shear flow, consider a numerical particle that, at the beginning of a time step, is located at $\mathbf{x}(t = 0) = \mathbf{x}_0$. The combined effect of shear advection and diffusion is expressed by a random jump of the particle to a new location at time t . We define f as the probability density function (PDF) of the new location, neglecting reaction. By definition, f is the solution of the advection-diffusion equation

$$\frac{\partial f}{\partial t} + \alpha y \frac{\partial f}{\partial x} = \frac{1}{\text{Da}} \nabla^2 f, \quad (12)$$

for natural boundary conditions (i.e. $f \rightarrow 0$ and $\nabla f \rightarrow 0$ as $\mathbf{x} \rightarrow \infty$) and initial condition $f(\mathbf{x}, t = 0) = \delta(\mathbf{x} - \mathbf{x}_0)$. Hence, f is the fundamental solution of (12). It is given by the multivariate Gaussian [40, 45]

$$f(\mathbf{x}, t; \mathbf{x}_0) = \frac{1}{(2\pi)^{d/2} \sqrt{\det[\boldsymbol{\kappa}]}} \exp \left[-\frac{1}{2} \boldsymbol{\xi}^T \boldsymbol{\kappa}^{-1} \boldsymbol{\xi} \right] \quad (13)$$

with a covariance matrix given by

$$\boldsymbol{\kappa} = \boldsymbol{\kappa}(t) = \frac{2t}{\text{Da}} \begin{bmatrix} 1 + (\alpha t)^2/3 & \alpha t/2 \\ \alpha t/2 & 1 \end{bmatrix} \quad (14)$$

where

$$\boldsymbol{\xi} = \mathbf{x} - (\mathbf{x}_0 + \alpha y_0 t \hat{\mathbf{x}}) \quad (15)$$

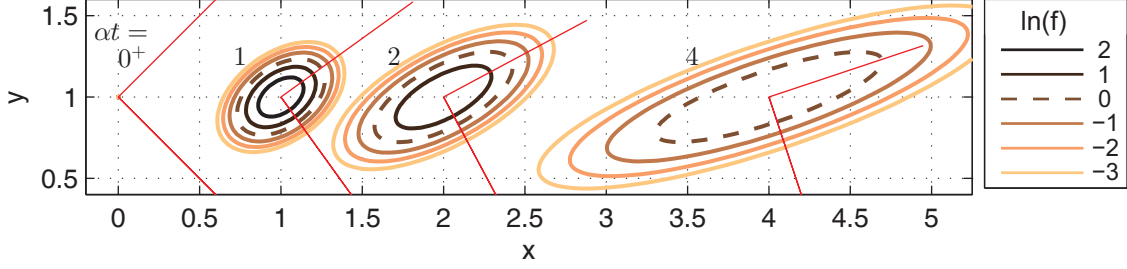


FIG. 1. (Color online) Illustration of the temporal evolution of the spatial PDF (log scale) and the eigenvectors of κ for a passive particle transported by shear flow.

is the offset from the mean location, $y_0 = \mathbf{x}_0 \cdot \hat{\mathbf{y}}$ is the initial y -coordinate, and $\hat{\mathbf{x}}, \hat{\mathbf{y}}$ are the unit vectors in the x, y directions, respectively. Iso-contours of the distribution are rotated ellipses with common foci at $\mathbf{x}_0 + \alpha y_0 t \hat{\mathbf{x}}$ (See figure 1). The principle axes of the ellipses are aligned with the eigenvectors of κ , and rotate with time due to shear; one axis is growing super-diffusively and the other diffusively. Note that when $\alpha \rightarrow 0$, the distribution (13) converges to the $2d$ axi-symmetric Gaussian (the fundamental solution of the ADE with constant diffusion). Further details on the implementation of this method, as well as analytical expressions for the eigenvalues and eigenvectors κ are provided in Appendix A.

B. Reaction

Next, based purely on transport, we wish to determine if two particles that are initially separated at $t = 0$ will collocate, and thus potentially react, over the next time step. Consider two particles, one of species A and the other of species B , that are located at $\mathbf{x}_A, \mathbf{x}_B$ initially at $t = 0$. The temporal density of their probability to collocate over some infinitesimal volume $d\mathbf{x}$ at time t is obtained by the product of their respective random walk PDFs and $d\mathbf{x}$. Thus, the temporal density of their probability to collocate in *any* position in space is given by an integral over this product,

$$v = \int f(\mathbf{x}, t; \mathbf{x}_A) f(\mathbf{x}, t; \mathbf{x}_B) d\mathbf{x} \quad (16)$$

where integration is taken over the entire space. This expression is a convolution of two Gaussians, and is itself equal to a Gaussian with the sum of variances,

$$v(\mathbf{s}, t) = \frac{1}{2\pi\sqrt{\det[\boldsymbol{\kappa}_A + \boldsymbol{\kappa}_B]}} \exp\left[-\frac{1}{2}\mathbf{s}^T(\boldsymbol{\kappa}_A + \boldsymbol{\kappa}_B)^{-1}\mathbf{s}\right] \quad (17)$$

where $\mathbf{s} = \mathbf{x}_A - \mathbf{x}_B$ is the distance between the particles at time $t = 0$. The convolution in (16) which yields (17) can be performed in Fourier space via the *Faltung* theorem [54]. Since $\boldsymbol{\kappa}_A = \boldsymbol{\kappa}_B = \boldsymbol{\kappa}$ we can rewrite (17) as

$$v(\mathbf{s}, t) = \frac{\text{Da}}{8\pi t\sqrt{1 + (\alpha t)^2/12}} \exp\left[-\frac{\text{Da}(|\mathbf{s}|^2 - s_x s_y \alpha t + s_y^2 (\alpha t)^2/3)}{8t(1 + (\alpha t)^2/12)}\right]. \quad (18)$$

where $|\mathbf{s}| = \sqrt{s_x^2 + s_y^2}$. We thus see that the collocation probability density (18) depends on the following parameters: (1) both components of \mathbf{s} , the initial inter-particle distance, (2) the diffusion length scale $(2t/\text{Da})^{1/2}$, and (3) the characteristic distance due to shear, αt .

Assuming that the pair of A, B particles has survived over time t (i.e. they have not reacted with other particles), their probability to react with each other during the infinitesimal time $t' \in [t, t + dt)$ is given by

$$m_p v(\mathbf{s}, t) dt, \quad (19)$$

where m_p is the non-dimensional mass carried by a single particle, i.e. the number of moles multiplied by l^2/C_0 . Thus, the probability of survival is given by the conditioned probability

$$P_s(t + dt) = P_s(t)[1 - m_p v(\mathbf{s}, t) dt], \quad (20)$$

or, in words, the probability they are unreacted at $t + dt$ is the probability they were unreacted at t and did not react with each other since then. Hence,

$$dP_s/P_s = -m_p v(\mathbf{s}, t) dt \quad (21)$$

and by integration over a time step t , we obtain the overall reaction probability of the couple during that time step,

$$P_r(t) = 1 - P_s(t) = 1 - \exp\left[-m_p \int_0^t v(\mathbf{s}, t') dt'\right]. \quad (22)$$

For the degenerate case $\alpha = 0$, the integral in (22) yields

$$\int_0^t v(\mathbf{s}, t') dt' = \frac{\text{Da}}{8\pi} \text{E}_1\left(\frac{\text{Da}}{8t} |\mathbf{s}|^2\right), \quad (23)$$

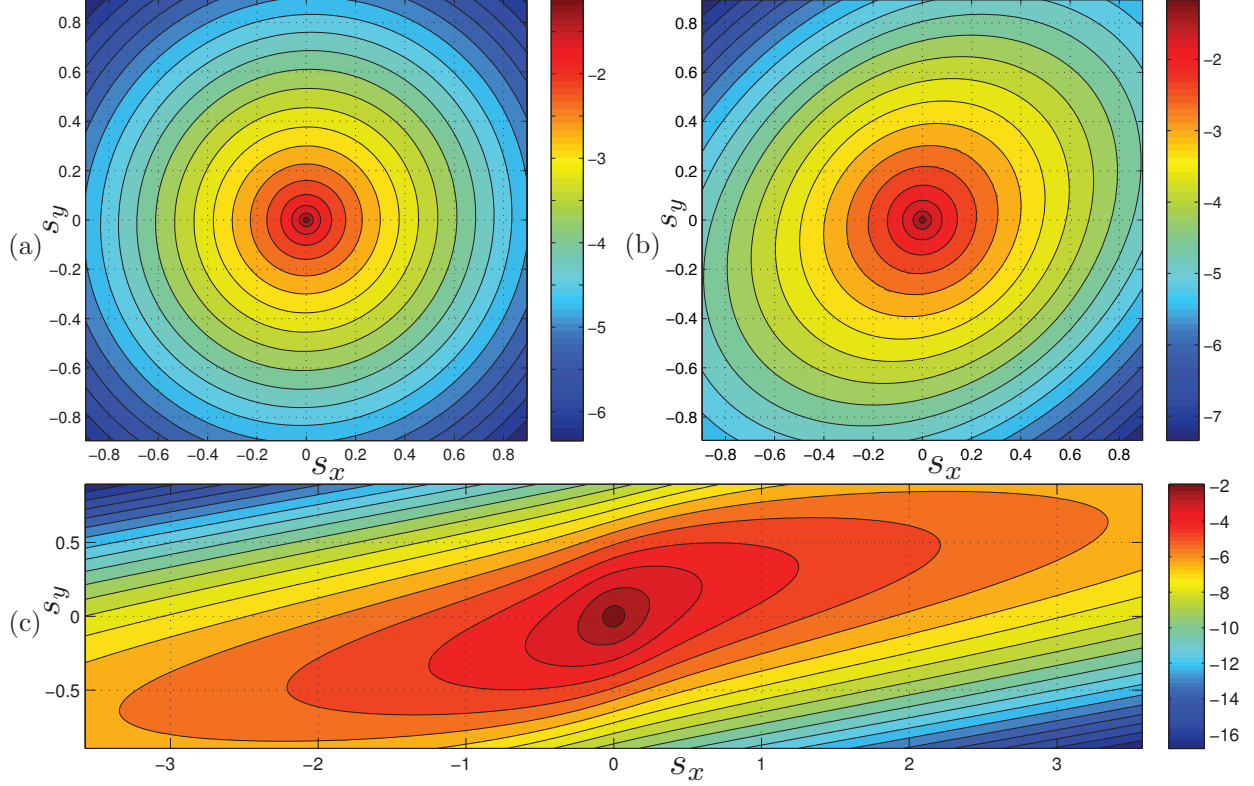


FIG. 2. (Color online) The integrated non-dimensional collocation probability $\int_0^t v(\mathbf{s}, t') dt'$ (in log scale) for $\text{Da}/t = 1$ and $\alpha t = 0.1, 1, 10$ in (a), (b), (c) respectively.

where E_1 is the exponential integral. Note how this expression depends only on the absolute value of the inter-particle distance, as the system becomes isotropic when $\alpha = 0$. For the general case $\alpha \neq 0$, equation (22) is integrated numerically (fig. 2). However, the simplified solution (23) can be useful for approximating (22) when $(\alpha t)^2 \ll 12$. Hence, it can be used if the time steps are small enough (recall that t is the length of the time step in the framework of this section).

Also, with (23) it is easy to see that if $\frac{\text{Da}}{8t} s^2 \rightarrow 0$, then the integral in (22) tends to infinity, and $P_r \rightarrow 1$. This comes as no surprise: when the particles are close by, or when they are given enough time to diffuse, their collocation probability is expected to be close to 1.

If, on the other hand, $t \rightarrow 0$, while $\mathbf{s} \neq 0$, the collocation probability tends to a Delta function in \mathbf{s} , and $P_r \rightarrow 0$. Again, this is expected, since particles that are sufficiently far from one another cannot collocate unless they are given sufficient time to diffuse.

From a practical perspective to reduce numerical costs, the search for neighbours must

256 be limited to a certain distance range. We define this range by the ellipse

$$\mathbf{s}^T(2\boldsymbol{\kappa})^{-1}\mathbf{s} = 2a^2 \quad (24)$$

257 where $a > 0$ is some predefined constant. Choosing larger a improves the accuracy of the
 258 numerical approach, but has an increased computational cost; as a rule of thumb, the choice
 259 $a = 2$ is typically sufficient as any induced error will be insignificantly small[51]. Note again
 260 that when $\alpha = 0$ the ellipse converges to a circle of radius $a\sqrt{8t/\text{Da}}$.

261 With this cut-off search distance, the collocation probability (17) integrates to

$$\eta = 1 - e^{-a^2}, \quad (25)$$

262 so the collocation probability needs to be rescaled by the factor η^{-1} for consistency to ensure
 263 integration over the density to be unity. Hence, the probability of reaction of a single A
 264 particle during a time step is evaluated by numerical integration of (22), or by the first order
 265 approximation

$$P_r = \eta^{-1}m_pt \sum_{i=1}^{N_{nb}} v(\mathbf{s}_i, t) \quad (26)$$

266 where N_{nb} is the number of B neighbours found within the ellipse. The probability is
 267 compared to a random number generated from a uniform distribution $U \in [0, 1]$. If $U > P_r$,
 268 the A particle under consideration is annihilated (removed from the system), and one of
 269 the neighbouring B particles is annihilated as well. The choice between neighbours is done
 270 based on their weighted probability of reaction, so that we randomly choose the B particle
 271 based on its relative probability of reaction. Additionally if a naïve search is performed
 272 to calculate collocation probabilities between all product pairs in the system, this can be
 273 computationally costly at $O(N^2)$, where N is the number of particles used. To speed up
 274 this process we use an algorithm from the data mining literature called the kd -tree [55],
 275 which accelerates this search to an $O(N \log N)$ process, providing significant computational
 276 savings.

277 C. The numerical domain and finite size effects

278 The system we consider is idealized as ergodic and infinite. Therefore, the total mass
 279 in the system is infinite as well. Each particle represents a finite mass m_p . Hence, the

number of particles needed to simulate the system accurately is infinite. This is clearly unfeasible, since the number of particles in a numerical particle tracking simulation is finite and inherently constrained by the computational resources. To overcome this difficulty, we follow the classical approach of simulating the infinite system over a finite domain with periodic boundary conditions. At early times of the simulation, the finiteness of the domain is expected to have a negligible effect on the results and the domain can be considered infinite. However, at late times, boundary effects in the numerical simulation will lead to deviations from this idealisation.

Indeed, previous works on purely diffusive transport [21, 23, 51] have observed and discussed this effect. For the case of no shear ($\alpha = 0$) over a domain of non-dimensional size Ω^d with periodic boundary conditions the finite size effects kick in when the typical size of segregated islands grows to about half of the domain size. This was observed around the time

$$t_{bnd} = \text{Da}(\Omega/8)^2 \quad (27)$$

which can be thought of as representing the characteristic time of diffusion of concentration perturbations over the finite simulation domain. Similar if not more restrictive conditions will arise when $\alpha \neq 0$ and will be discussed in greater detail below. In this study, we use a rectangular domain $\mathcal{S} : [0, \Omega_x] \times [0, \Omega_y]$ for the numerical simulation.

D. Implementation of initial conditions

Implementing periodic boundary conditions in a numerical particle tracking method over a rectangular domain is straightforward. The initial conditions (9-11) were implemented by randomly spreading N_0 particles of each species in the domain \mathcal{S} . The number of particles is not arbitrary, but rather is derived from the initial condition. Let us define the initial non-dimensional density of particles by

$$\rho_0 = N_0/(\Omega_x\Omega_y). \quad (28)$$

This particle density is inversely proportional to the magnitude of the initial white noise μ and given by

$$\rho_0 = 1/\mu. \quad (29)$$

305 This expression is a straightforward extension of the one derived by Paster *et al.* [51, Ap-
 306 pendix C]. To understand this result, consider a system where the initial condition for
 307 $C_i(\mathbf{x}, t = 0)$ is deterministic, i.e.

$$C_A(\mathbf{x}, t = 0) = C_{A0}(\mathbf{x}) , C_B(\mathbf{x}, t = 0) = C_{B0}(\mathbf{x}), \quad (30)$$

308 such that $\mu \rightarrow 0$ (zero noise term). By (29), we find $\rho_0 \rightarrow \infty$. Hence, even if the domain is
 309 finite, an exact representation of the initial condition (30) necessitates the use an of *infinite*
 310 number of particles, which is consistent with classical random walk theory [56]. For such
 311 case, a particle tracking algorithm may be less favourable due the error induced by the finite
 312 number of particles.

313 In contrast, if we are interested in the case of a noisy/stochastic initial condition, as is the
 314 case with the present work, this method might be regarded as ideal. For such cases, particle
 315 tracking methods require a finite number of particles for an accurate representation of the
 316 initial condition. When the initial condition contains a considerable noise, the reactive
 317 particle tracking method may be very efficient with regard to computational resources,
 318 due to the small number of initial particles needed. This may be an advantage over other
 319 numerical methods, such as Monte Carlo simulations using Eulerian finite difference, volume
 320 or element methods. Additionally, random walk methods are known to be much less prone
 321 to numerical diffusion, which would lead to greater mixing and is thus an important factor
 322 in mixing-driven reactions[57].

323 V. RESULTS

324 Using the numerical algorithm described in the previous section, we have performed
 325 various simulations to study the effect of the Dahmköler number (Da) and shear rate (α)
 326 on the evolution of average concentration in the system (table I). In figure 3 we show
 327 representative results for a specific Dahmköler number, namely $Da = 2$, spanning a range of
 328 α values ($0, 10^{-4}, 10^{-3}, 10^{-2}, 10^{-1}, 1, 10$). The figure also shows two analytical solutions,
 329 one corresponding to the well-mixed case, and an approximate analytical solution [51] that
 330 incorporates noisy initial conditions for $\alpha = 0$. A slight discrepancy between the numerical
 331 and the approximate analytical solution for $\alpha = 0$ is observed. As discussed in further
 332 detail in the following section, this discrepancy is due to restrictive assumptions involved

Da	α	N_0	Δt_0	ϵ	Δt_{max}
2	0	6.4×10^6	2.5×10^{-3}	10^{-2}	50
	10^{-4}		2.5×10^{-3}	0.01	10
	10^{-3}		2.5×10^{-3}	0.01	10
	10^{-2}		2.5×10^{-3}	0.01	1
	10^{-1}		2.5×10^{-3}	0.01	1
	1		10^{-3}	2.5×10^{-3}	0.25
	10		2.5×10^{-4}	2.5×10^{-3}	0.05
8	0	1.6×10^6	0.025	0.025	100
	10^{-4}		0.025	0.025	100
	10^{-3}		0.025	0.025	100
	10^{-2}		0.025	0.025	10
	10^{-1}		0.025	0.025	10
	1		0.012	0.012	5
	10		0.012	0.012	1

TABLE I. Parameters of the numerical simulations. To speed up runs, the time step size is given by $\Delta t_j = \min\{\Delta t_{\max}, \Delta t_0(1 + \epsilon)^j\}$, where j is the step number. For all simulations, $t_{bnd} = \text{Da}N_0/64 = 5 \times 10^4$, the number of ensemble realizations was $N_{sim} = 8$, the search radius factor was $a = 2$, and domain size was $\Omega_x \times \Omega_y = 1 \times 4$.

in developing the analytical solution, namely the neglecting of high-order moments of the concentration fluctuation fields.

A. Pure diffusion: $\alpha = 0$

First, to elucidate some matters, let us focus on the previously studied case of pure diffusion and no shear ($\alpha = 0$). The mean concentration curve for this case (see figure 3) matches the well-mixed solution at very early times, but clearly diverges from the well-mixed solution at relatively early times. This is consistent with the noisy initial condition for concentration, and has been extensively discussed in previous works (e.g. Paster *et al.* [51] and references therein). For this case, the only mixing mechanism is diffusion, which

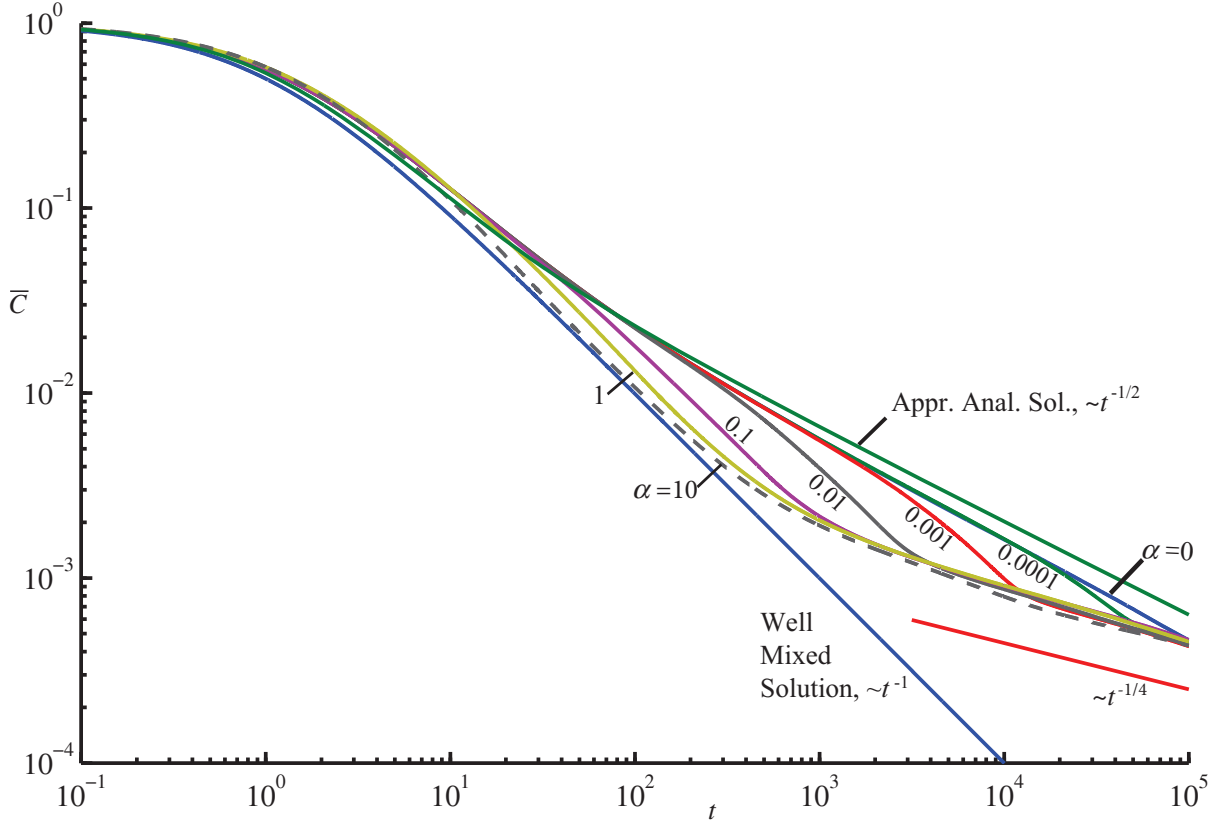


FIG. 3. (Color online) The evolution of mean concentration with time for $Da = 2$. The approximate analytical solution for $\alpha = 0$ and the well-mixed solution are also plotted. All parameters are non-dimensional.

strives to homogenize the concentration field and drive the system to a well-mixed state. At the same time, reaction occurs in all locations where A and B coexist, thus annihilating A and B and promoting the segregation of species, destroying mixing in the system. Figure 4 depicts snapshots of particle locations at various times during the course of the simulation. These reveal that at very early times, A and B particles largely overlap in space and the system can be regarded as relatively well-mixed. At later times segregation leads to the formation of the aforementioned islands of single species, and reactions become restricted to their boundaries. At times for which island segregation is clearly visible, the average concentration in the domain scales with time as $t^{-1/2}$, in agreement with previous predictions and observations. As seen in figure 4, the total number of islands decreases with time, and the average size of an island grows respectively. Islands that contain significant mass of one species consume neighbouring islands with lower mass of the second species, which in turn

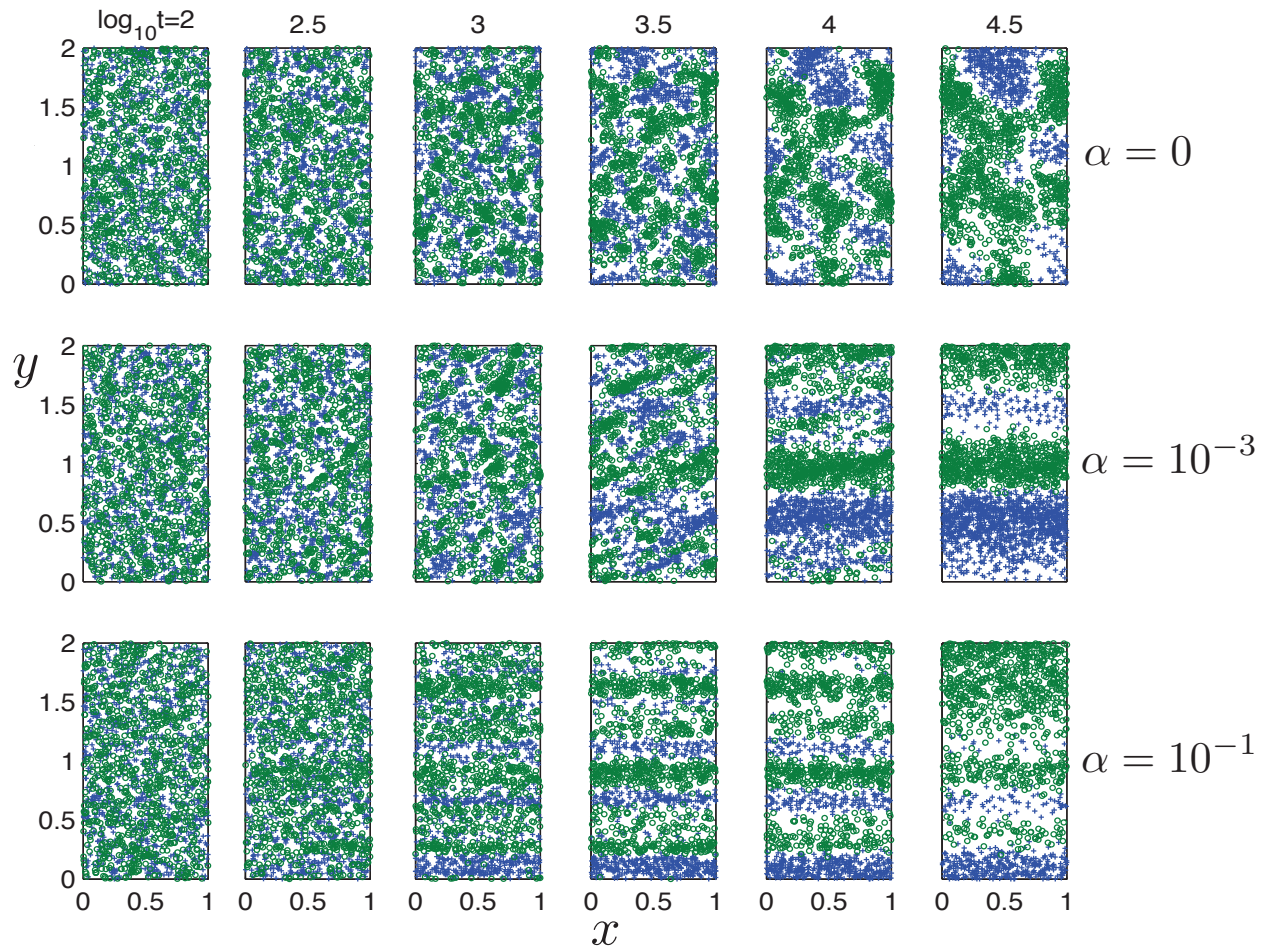


FIG. 4. (Color online) Evolution in time of some representative realizations with various shear rates, for $Da = 2$. Note how the islands form initially with irregular shape. Later on, for $\alpha > 0$, they tilt and become elongated due to the shear, and finally lie flat perpendicular to the x -axis. Compare with figure 3. Note that, in the above figures, particle numbers were reduced (randomly) to $\sim 10^3$ to allow a good visualization of the results, and only the bottom half of the domain is shown.

disappear from the system. At very late time, around $t \simeq t_{bnd}$ (see equation (27)), the finite size of the numerical domain starts to affect the simulation. At this time, the area occupied by a single island reaches about half the domain area and the infinite-domain behaviour breaks down. As noted above, for a detailed discussion on this see [51].

B. Diffusion and shear: $\alpha \neq 0$

For the cases where shear effects do exist (i.e. $\alpha \neq 0$), we observe a different behaviour from the purely diffusive case, highlighting the role that shear plays in this system. Up to four discernible time regime scalings in average concentration emerge, which will be discussed in detail. First we qualitatively describe the results.

At very early times, in all cases, there is a close agreement between the zero shear and finite shear simulations; at these earliest times diffusion dominates over shear effects and the latter are not discernible in the mean behaviour of the system. At these times the solutions break away from the well-mixed case and, other than for the highest simulated shear cases, all display the $t^{-1/2}$ regime. In the largest shear case ($\alpha = 10$), shear effects are strong enough to suppress this regime and the solution closely follows the well-mixed prediction, indicating that large shear can indeed suppress incomplete mixing effects. Then at some α -dependent time, the solutions break away from this scaling and shift to a faster scaling of t^{-1} . The larger α , the earlier this transition occurs. During this time the concentration evolves parallel to the well-mixed solution, but at higher overall concentrations. Then again at some α -dependent value the solutions break away from this scaling and transition to another slower scaling of $t^{-1/4}$. This is a finite size effect associated with the horizontal size of the domain, which is unavoidable in a numerical study and can be explained theoretically (see section VI), but is not expected in an infinite domain. All solutions collapse together during this regime, with deviations for different α values well within the standard deviation of the Monte Carlo simulation. Not surprisingly, we observed that increasing the number of realizations to calculate the average concentrations reduced the magnitude of these deviations. Since we are primarily interested in infinite-domain effects, we will focus on the regimes before the shear- and diffusion-induced boundary effects take place. Nonetheless the latter warrant some further discussion.

Figure 4 shows particle locations at various times during the simulations for the $Da = 2$ case for multiple values of α . What is interesting to note is that at early times when the mean concentrations still match the $\alpha = 0$ case (see figure 3), the generic shapes of the islands look very similar to the $\alpha = 0$ case regardless of the specific value of α . However as the breakaway from this regime occurs to the faster t^{-1} scaling, a noticeable difference appears, whereby the islands take on a different shape. At these times the islands are more elongated in one

direction, which is tilted relative to the natural y axis, reflecting the presence of shear in the system and the fact that there is a super-diffusive growth along one axis and a diffusive one along the other. This is directly analogous to the fundamental solution of a point source in a diffusive shear flow in equation (13). It is at these times that the effect of the shear flow is important in the system.

Next, during the $t^{-1/4}$ regime (the finite size effect scaling), all islands now span the full horizontal extent of the domain. In essence they have tilted all the way such that the super-diffusively growing axis is now closely aligned with the x axis. Reactions are now mostly limited by vertical diffusion across islands and the system behaves as if it were one-dimensional, which is consistent with an incomplete mixing scaling of $t^{-d/4}$ with d , the number of spatial dimensions, equal to one. This is a finite size effect associated with the time it takes for an island to span the horizontal width of the domain, unavoidable in a finite size numerical simulation, but not expected in an infinite domain (see the following section and Appendix B for more discussion and explanation on the matter).

Finally at t_{bnd} (see equation (27)) another finite size effect, the same as in the cases with no shear, kicks in. At this point the islands occupy half the domain; there is no longer any space for islands to grow as they would in an infinite domain, and a complete breakdown occurs. It is interesting to note that at the latest time in all the shear flow cases the islands are horizontally elongated, again reflecting the role of shear, while for the pure diffusion case it is equi-probable that they could be vertically or horizontally aligned, as there is no preferential direction for growth in a purely diffusive system.

Figure 5 shows the mean concentration against time for the same $Da = 2$ as well as $Da = 8$. This figure serves to highlight that qualitatively the behaviour for both Da is very similar and all the observations and scalings discussed above still emerge. However, the breakaways from the well-mixed behaviour and transitions between each of these scaling regimes occur at different times, indicating a Da -dependent behaviour also. The emergence of these distinct time scalings is key to understanding incomplete mixing effects on chemical reactions, but at this point it is difficult to truly quantify these scalings from these observations alone. In the following, section VI, the results will be interpreted using a semi-analytical model that enables a more mechanistic explanation of each regime.

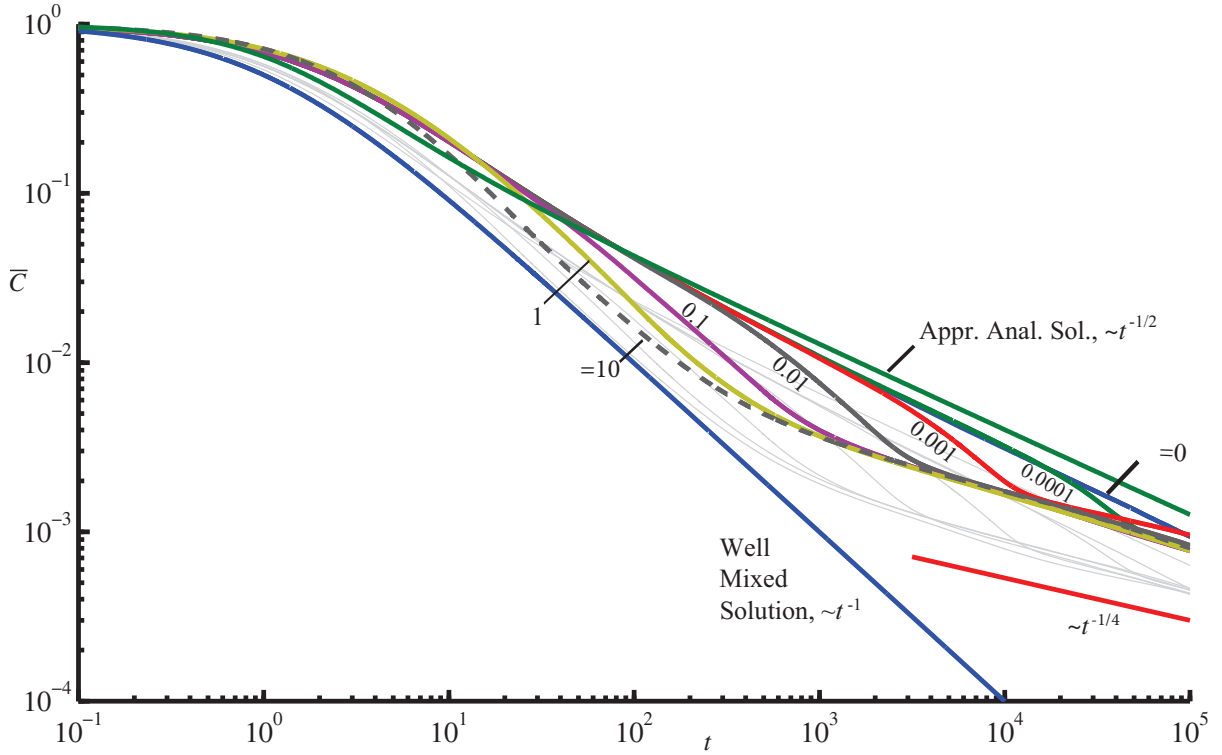


FIG. 5. (Color online) Same as figure 3 with additional solutions for $Da = 8$. The thin grey lines in the background correspond to the results for $Da = 2$.

VI. INTERPRETATION OF SIMULATION RESULTS - A SEMI-ANALYTICAL CLOSURE

In this section we present a semi-analytical solution, based on methods from previous works that look at purely diffusive transport, to explain each of the time scaling regimes for mean concentration that were observed in section V. This semi-analytical approach is based on a closure argument. Similar closures have been invoked in many previous studies, but it should be noted that it is known to not be exact [18, 21–23]. Rather, it enables one to predict the emergent scalings with time of mean concentrations, but not the exact values of mean concentration or time when these occur. Even in purely diffusive cases it is unable to match observations exactly without some empirical correction. These discrepancies have been studied and explained in detail by Paster *et al.* [51]. This is due to a problematic assumption behind the derivation of the closure, discussed below. Given these well known limitations, our objective here is not to match exactly the observations from the numerical

simulations, but to explore the emergent scalings with such a closure.

A. Closure Problem for Mean Concentrations

Averaging over equations (1)–(3) it can readily be shown that the mean concentration of the reactants in this system will evolve based on the following ordinary differential equations

$$\frac{d\overline{C_A}(t)}{dt} = \frac{d\overline{C_B}(t)}{dt} = -\overline{C_A}^2 - \overline{C'_A C'_B}. \quad (31)$$

Here we have used the physical requirement that $\overline{C_A}(t) = \overline{C_B}(t)$ at all times, since the initial condition is $\overline{C_A}(t=0) = \overline{C_B}(t=0)$ and the reaction stoichiometry is 1:1. When fluctuation concentrations are small relative to mean concentrations, the second term on the right hand side of (31) will be negligible and the system will evolve as is if it were well-mixed. However, when the fluctuations are not small relative to mean concentrations this term plays an important role, changing the evolution of the system in a meaningful manner. This presents a closure problem as it requires a governing equation or model for the $\overline{C'_A C'_B}$ term.

To close this problem we rely on previous works in diffusive and super-diffusive systems, where using the method of moments it has been shown that a reasonable closure is to assume

$$\overline{C'_A C'_B} = -\chi G(\mathbf{x} = \mathbf{x}_{peak}, t), \quad (32)$$

where G is the Green's function for conservative transport in the specified system, \mathbf{x}_{peak} is the location of the peak of the Green's function, and χ is a constant. The formal derivation of closure (32) can be found in refs. 23, 58, and 59, where exact expressions for χ are developed. Similar closures without formal derivation have been proposed [18, 22]. However, it is important to note that it relies on the assumption that moments higher than third order (i.e. terms that consist of products of three fluctuation concentrations) are negligible. While this is a standard assumption in many closure problems it is inaccurate as highlighted by Paster *et al.* [51], who showed that in diffusive systems the semi-analytical solution and high resolution numerical solutions, while qualitatively similar in the late time scaling, will behave differently. Indeed, using the 'exact' values predicted by neglecting higher order moments [23, 58] can in some instances yield unphysical results (e.g. creating rather than destroying mass of reactants when χ is too large). This mismatch is reconciled by demonstrating that

third and higher order moments are in fact not negligible, but can have similar structure to second order moments, manifesting as a different effective value of χ [51]. This justifies the structure of closure (32), but not the specific value of χ predicted. Thus, for now, we keep χ as a free (constant) parameter in our closure.

B. Green's function for pure shear flow

The Green's function for transport in a pure shear flow, within our dimensionless framework, satisfies the following governing equation

$$\frac{\partial G}{\partial t} + \alpha y \frac{\partial G}{\partial x} = \frac{1}{\text{Da}} \nabla^2 G \quad (33)$$

with natural boundary conditions at infinity and initial condition

$$G(\mathbf{x}, t = 0) = \delta(\mathbf{x} - \mathbf{x}_0), \quad (34)$$

in full analogy with the problem posed by (12), whose solution is given by (13). Thus

$$G(\mathbf{x} = \mathbf{x}_{peak}, t) = \frac{1}{2\pi\sqrt{\det[\boldsymbol{\kappa}]}} = \frac{\text{Da}}{2\pi t\sqrt{4 + (\alpha t)^2/3}}. \quad (35)$$

Perhaps most notable in this solution is that for small α or small times the leading order behaviour of $G(\mathbf{x} = \mathbf{x}_{peak}, t)$ scales like t^{-1} , but at sufficiently large times, when the α -dependent term dominates in the denominator, the leading behaviour scales like t^{-2} , which reflects the hypermixing regime alluded to earlier, where the plume spreads and the concentration peak decreases super-diffusively.

C. Solutions with the closure

With the proposed closure (32) and (35), our governing equation for the mean concentrations of the reactants (31) becomes

$$\frac{d\overline{C_A}(t)}{dt} = -\overline{C_A}^2 + \frac{\chi \text{Da}}{2\pi t\sqrt{4 + (\alpha t)^2/3}}. \quad (36)$$

While we are not aware of a closed form analytical solution to this equation for $\alpha \neq 0$, it is straightforward to integrate it numerically. Additionally, some useful asymptotic arguments can be made to understand how the solution evolves in time. These are discussed

in the following subsection. Then, to show the full emergent behaviour and verify our asymptotic arguments, we present numerical solutions of this equation. Note that for $\alpha = 0$ equation (36) is a Riccati equation whose solution can be expressed in terms of Bessel functions [21, 23].

Early times - At early times, if the background fluctuations in concentration are small relative to mean concentration we expect the dominant balance in equation (36) to be between the term on the left hand side and the first term on the right hand side. In this case the equation can be solved as

$$\overline{C}_A(t) = \frac{1}{1+t} \quad (37)$$

which is the solution for the well-mixed system.

Late times - As the concentrations deplete, the term $d\overline{C}_A/dt$ in equation (36) becomes negligible compared to the other terms in the equation. Then, the dominant balance in the equation shifts and becomes a balance between the two terms on the right hand side. Thus

$$\overline{C}_A = \left(\frac{\text{Da}\chi}{2\pi t \sqrt{4 + (\alpha t)^2/3}} \right)^{\frac{1}{2}} = \left(\frac{\text{Da}\chi}{4\pi} \right)^{\frac{1}{2}} (t^2 + \alpha^2 t^4/12)^{-\frac{1}{4}}. \quad (38)$$

Late time scaling 1 - Now if at these times $t^2 \gg \alpha^2 t^4/12$, or $t < \sqrt{12}/\alpha$, then to leading order the concentration will decrease as $\overline{C}_A \sim t^{-1/2}$, which is the same scaling one would obtain for a purely diffusive system at late times in two dimensions. Note that for large values of α this intermediate condition is not necessarily met, since it may be violated when the incomplete mixing effects become important. Indeed for the $\alpha = 10$ cases presented in figure 5 this scaling never emerges.

Late time scaling 2 - At larger times when $\alpha^2 t^4/12 \gg t^2$, or $t > \sqrt{12}/\alpha$, the concentration will scale as $\overline{C}_A \sim t^{-1}$, which is the same scaling as if the system were well-mixed. This suggests that the effect of a pure shear flow can indeed be strong enough to overcome the effects of incomplete mixing. However, the overall concentrations in the system could be considerably larger than the purely well-mixed case, due to the intermediate $\overline{C}_A \sim t^{-1/2}$ regime.

In a well-mixed system, the solution will evolve as $1/(1+t)$, which at late times approaches t^{-1} . Thus we can define an asymptotic late time retardation factor,

$$R_{asy} = \left(\frac{2\pi\alpha}{\sqrt{3}\text{Da}\chi} \right)^{\frac{1}{2}}, \quad (39)$$

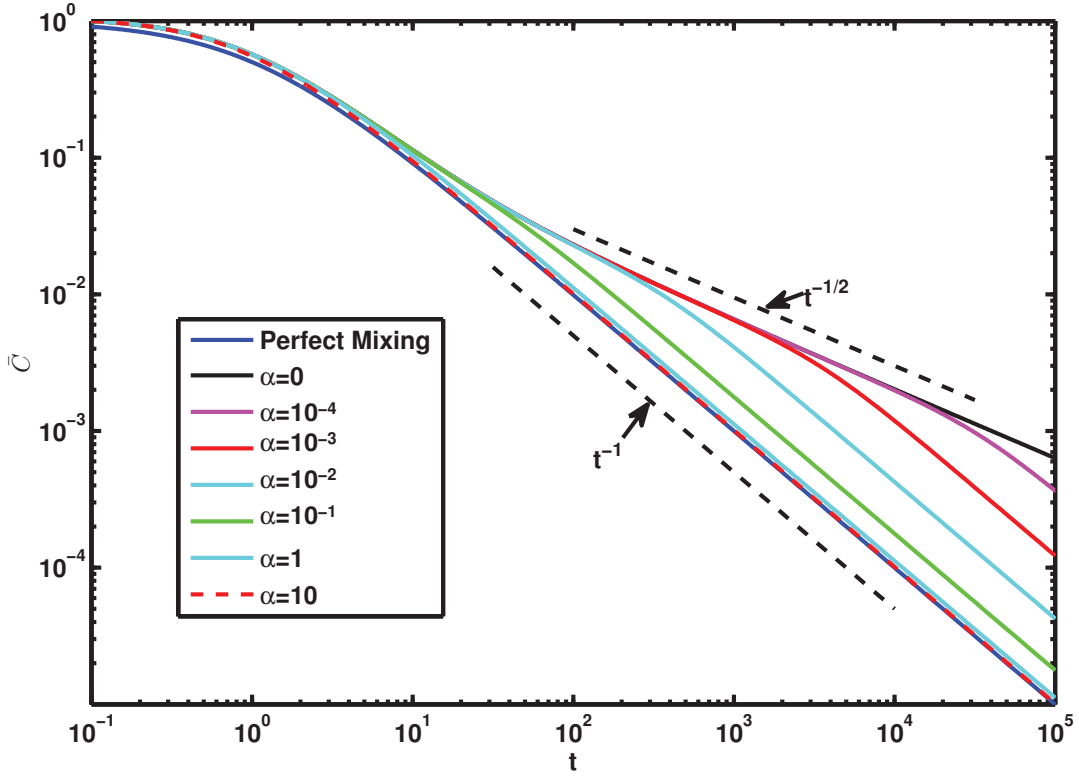


FIG. 6. (Color online) Numerical solution of (36) for various α , with fixed $\text{Da}\chi = 5 \times 10^{-1}$. At late times, concentration scales like $t^{-1/2}$; at even later times, if $\alpha \neq 0$, it scales like t^{-1} . The value of α affects the time of transition between each of the scaling regimes.

such that the concentration converges to $(R_{asy}t)^{-1}$, i.e. the influence of shear is to return the system to behaving in a manner reflective of perfect mixing, but at a later time. This is equivalent to having an effective (retarded) reaction rate $k_{eff} = k/R_{asy}$. While the notion of an effective reaction rate at these late times is useful, note that it should only be applied at late times when $t > \sqrt{12}/\alpha$.

1. Numerical solutions of semi-analytical equation

In this section we solve equation (36) numerically, using the numerical ordinary differential equation solver `ode23` available in MATLAB. From (36) it is evident that $\overline{C}_A(t)$ is a function of time depending on $\text{Da}\chi$ and α . Results varying and showing the respective influence of these are shown in figures 6 and 7.

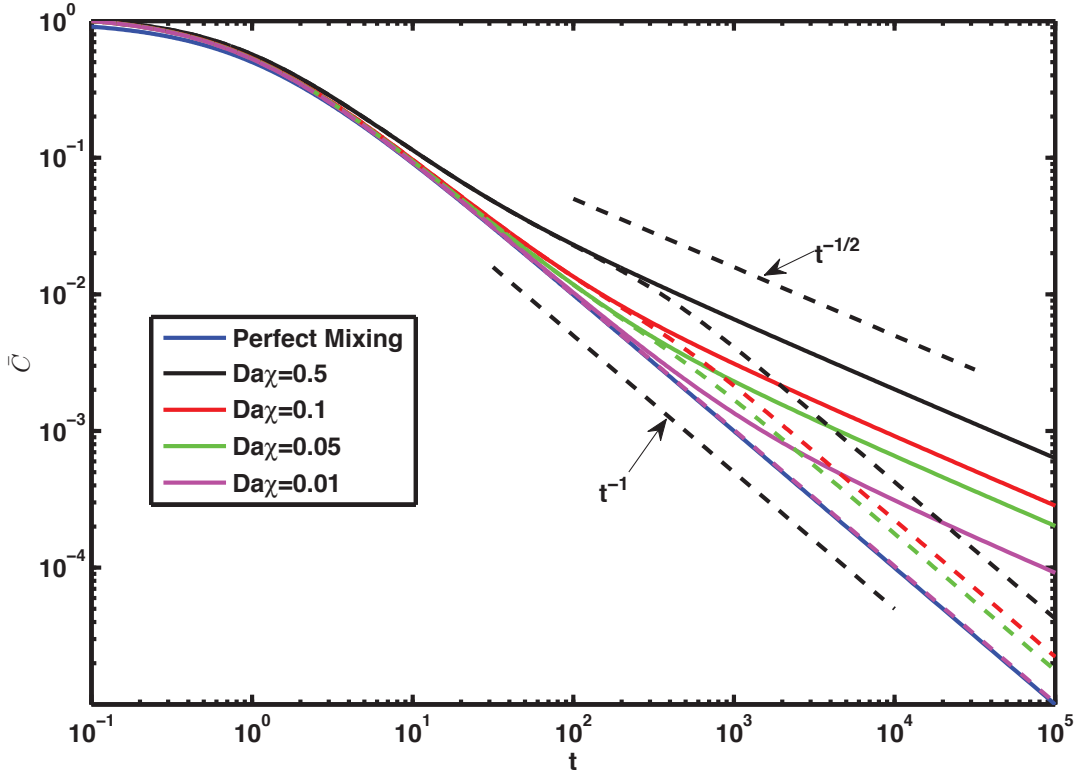


FIG. 7. (Color online) Numerical solution of (36) for various $\text{Da}\chi$. In this figure $\text{Da}\chi$ is varied to show how it affects the transition between each of the scaling regimes. The solid lines correspond to the equivalent case with no shear, i.e. $\alpha = 0$, and the dashed lines to $\alpha = 10^{-2}$.

In figure 6 we consider fixed $\text{Da}\chi$ and vary α over several orders of magnitude to demonstrate the influence of shear. In all cases at very early times we observe close agreement between the $\alpha = 0$ incomplete mixing solution and the solutions with shear. Then, again in all cases the solutions break away from this to a faster t^{-1} scaling as anticipated from the asymptotic arguments presented above. Larger α means an earlier breakaway to this faster regime. Note that the $\alpha = 10$ case never seems to follow the intermediate $t^{-1/2}$ regime, consistent with the idea that this regime need not occur if the conditions discussed above are not met.

In figure 7 we consider fixed α and vary $\text{Da}\chi$. In this figure the solutions for each $\text{Da}\chi$ combination and $\alpha = 0$ are also shown. Raising $\text{Da}\chi$ triggers incomplete mixing effects at earlier times. Larger χ suggests larger noise in the initial condition, while larger Da means higher ratio of reaction to diffusion. When the product is larger, this means that fluctuations

in the mean concentration will play an important role at earlier times. The effect of shear is to return from the $t^{-1/2}$ to a t^{-1} scaling. This is clearly seen for all cases and seems to occur at the same time, independent of $\text{Da}\chi$, which is again consistent with the arguments in the previous section since this transition is determined solely by the value of α .

For both figures 6 and 7 we do not observe the later time $t^{-1/4}$ scalings observed in the numerical simulations. As argued before, this scaling is a boundary effect due to the horizontal extent of the numerical domain, which an infinite domain solution cannot reproduce. Since our primary interest here is the influence of the initial conditions on the late time scaling of mean concentration in an infinite domain, we do not focus on the $t^{-1/4}$ scaling here. However, to demonstrate that it is truly a finite size effect associated with the limited horizontal extent of the domain we extend the current closure to include finite boundary effect in Appendix B, which consistently demonstrates this behavior.

VII. CONCLUSIONS

In this work we have studied mixing-limited reactions in a laminar pure shear flow to address the question of whether shear effects can overcome the effects of incomplete mixing on reactions. We have considered a simple spatial system, initially filled with equal amounts of two reactants A and B subjected to a background shear flow. The average concentrations of A and B are initially the same, but there are also background stochastic fluctuations in the concentrations. These can lead to long term deviations from well-mixed behaviours due to spatial segregation of the reactants, which can form isolated islands of individual reactants where reactions are limited to the island interfaces.

To study this system we adapted a Lagrangian numerical particle-based random walk model, built originally to study mixing-driven bimolecular reactions in purely diffusive systems, to the case with a pure shear flow with the long term goal of developing it for more general non-uniform flows. Additionally we studied the system theoretically by developing a semi-analytical solution approach by proposing a simple closure argument. The results of the two approaches are qualitatively analogous in that the mean concentrations of reactants over time scale with the same power laws. An exact quantitative match however is not obtained; it is well known from previous work on diffusive transport that such closures are not exact, but that they can match emergent scalings in mean concentrations, which we

demonstrate is also true for the case with shear considered here.

With both methods we observed the following behaviours. At early times, when mean concentrations are much larger than background fluctuations, the system behaves as if were well-mixed. Then, when the fluctuations become comparable in size to the mean concentrations, and the domain becomes segregated, incomplete mixing slows down the reactions. Thus, the mean concentrations in the system evolve with a slower characteristic temporal scaling, consistent with a diffusion-limited case where shear is absent. Then at later times when shear effects begin to dominate, the system returns to behaving in a manner similar to a perfectly mixed system, but described by an overall lower effective reaction rate constant. If shear is sufficiently strong, the diffusive-like incomplete mixing regime never emerges and the system behaves as well-mixed at all times. It is important to note that this does not mean that the system is actually well mixed as segregated islands still occur, but rather that the mixing associated with the shear flow is sufficiently fast to result in a scaling analogous to a well-mixed system.

The system is characterized by two dimensionless numbers. Da is a Damköhler number that quantifies the relative magnitude of reaction time scales to diffusion time scales. Large Da means that reactions happen more quickly than diffusion can homogenize any background fluctuations; thus systems with larger Da will amplify initial fluctuations and incomplete mixing patterns can play an important role at late times. Likewise, when Da is small, diffusion can homogenize fluctuations more quickly and the system will behave as better mixed. The second dimensionless number is α , a dimensionless shear rate that quantifies relative influence of shear to reaction. The Damköhler influences the onset time of incomplete mixing, while α controls the onset of a return to well-mixed type scaling.

A key take home message of this work is that, while a pure shear flow can lead to a behaviour that is consistent with a well-mixed system, if the nature and evolution of incomplete mixing in the system is not adequately accounted for, then predictions of reactant concentrations, particularly at late times, can be off by as much as orders of magnitude. In contrast, if incomplete mixing is accounted for, more realistic predictions can be obtained.

Appendix A: Expressions for the eigenvalues and eigenvectors of κ

The eigenvalues of κ , the covariance matrix, are given by

$$\lambda_{1,2} = \frac{1}{2} \left(\text{Tr}(\kappa) \pm \sqrt{(\text{Tr}(\kappa))^2 - 4 \det \kappa} \right) \quad (\text{A1})$$

where

$$\text{Tr}(\kappa) = \kappa_{11} + \kappa_{22} = \frac{4t}{\text{Da}} \left[1 + \frac{1}{6} \alpha^2 t^2 \right] \quad (\text{A2})$$

is the trace of κ and

$$\det \kappa = \kappa_{11} \kappa_{22} - \kappa_{12}^2 = \frac{4t^2}{\text{Da}^2} \left[1 + \frac{1}{12} \alpha^2 t^2 \right]. \quad (\text{A3})$$

Substituting (A2) and (A3) into (A1) one finds

$$\lambda_{1,2} = \frac{2t}{\text{Da}} \left[1 \pm \left(\frac{1}{2} \alpha t \sqrt{1 + \frac{1}{9} (\alpha t)^2} \right) + \frac{1}{6} \alpha^2 t^2 \right]. \quad (\text{A4})$$

The eigenvectors, in turn, are aligned with

$$\mathbf{v}'_{1,2} = \begin{bmatrix} 1 \\ -\frac{1}{3} \alpha t \pm \sqrt{1 + \frac{1}{9} (\alpha t)^2} \end{bmatrix} \quad (\text{A5})$$

and the normalized unit vectors $\mathbf{v}_{1,2}$ are readily obtained by normalization of $\mathbf{v}'_{1,2}$.

When $\alpha t \ll 1$, the eigenvectors are inclined at about $\pm 45^\circ$ relative to the \hat{x} axis. For larger αt , the eigenvectors tilt clockwise (see Fig. 1), and for $\alpha t \gg 1$, they tend to align with \hat{x} and $-\hat{y}$, or more precisely, with $(1, 3/(2\alpha t))$ and $(1, -\frac{2}{3}\alpha t)$.

In practice, the new location of a particle can be obtained by translation of the x coordinate of the particle by $\alpha y_0 t$, and a random walk in two dimensions with jumps along the rotated eigenvectors of κ with magnitudes:

$$\begin{aligned} x_1 &= \xi_1 \sqrt{\lambda_1} \\ x_2 &= \xi_2 \sqrt{\lambda_2} \end{aligned} \quad (\text{A6})$$

where x_i is the walk length in the direction of the i -th eigenvector, and ξ_i is a random number, generated from a normal distribution with zero mean and unit variance. Hence, the new location is given by

$$\begin{aligned} x &= x_0 + \alpha y_0 t + \sum_{i=1}^d (\mathbf{v}_i \cdot \hat{x}) x_i, \\ y &= y_0 + \sum_{i=1}^d (\mathbf{v}_i \cdot \hat{y}) x_i. \end{aligned} \quad (\text{A7})$$

Appendix B: Domain boundary effects

As discussed in section VI we wish to demonstrate that the $t^{-1/4}$ scaling can be attributed to a boundary effect. Specifically we will argue here that this scaling is associated with finite extent of the horizontal boundaries of the domain. As shown in equation (32) the evolution of the mean concentration depends on the peak of the Green's function for conservative transport. For a finite periodic domain this can be calculated by the method of images

$$G(\mathbf{x} = \mathbf{x}_{peak}, t) = \sum_{n=-\infty}^{\infty} \frac{1}{(2\pi)^{d/2} \sqrt{\det[\boldsymbol{\kappa}]}} \exp \left[-\frac{1}{2} \xi_n^T \boldsymbol{\kappa}^{-1} \xi_n \right], \quad (\text{B1})$$

where

$$\xi_n = (n\Omega_x, 0) \quad (\text{B2})$$

and Ω_x is the horizontal length of the domain. In essence this solution adds every contribution from point plumes located at equidistant intervals of Ω_x along the x-axis at $y = 0$ and sums their contribution to the point $x = 0$, which is where the peak of the Green's function for a point source located initially at $(x, y) = (0, 0)$ will occur. It is convenient to take this point as one does not have to account for advection induced drift in the peak location, but the result is independent of this choice. We have

$$G(\mathbf{x} = \mathbf{x}_{peak}, t) = \frac{\text{Da}}{4\pi t \sqrt{1 + \alpha^2 t^2 / 12}} \sum_{n=-\infty}^{\infty} \exp \left[-\frac{\text{Da}(n\Omega_x)^2}{4t(1 + \alpha^2 t^2 / 12)} \right] \quad (\text{B3})$$

which at late times converges to

$$G(\mathbf{x} = \mathbf{x}_{peak}, t) = \frac{\sqrt{3}}{2\pi} \frac{\text{Da}}{|\alpha| t^2} \sum_{n=-\infty}^{\infty} \exp \left[-\frac{3\text{Da}(n\Omega_x)^2}{\alpha^2 t^3} \right]. \quad (\text{B4})$$

The term outside of the summation scales like t^{-2} , as for the infinite domain case. As $t^3 \gg 3\text{Da}\Omega_x^2/\alpha^2$ when the boundary effects become important, the infinite sum can be approximated by an integral which converges to

$$\sqrt{\frac{\pi}{3\text{Da}\Omega_x}} t^{3/2}. \quad (\text{B5})$$

Thus, the Green's function converges to

$$G(\mathbf{x} = \mathbf{x}_{peak}, t \rightarrow \infty) = \frac{1}{2} \sqrt{\frac{\text{Da}}{\pi}} \frac{1}{\Omega_x} t^{-1/2}. \quad (\text{B6})$$

Hence, the combined effect on the scaling of the peak of the Green's function is

$$G(\mathbf{x} = \mathbf{x}_{peak}, t) \sim t^{-1/2}. \quad (\text{B7})$$

Since at late times our dominant balance argument indicates that $\overline{C}_i = \sqrt{\chi G(\mathbf{x} = \mathbf{x}_{peak}, t)}$, once the horizontal boundary effects are felt the mean concentrations will converge to

$$\overline{C}_i(t) = \sqrt{\chi G(\mathbf{x}_{peak}, t)} = \sqrt{\frac{\chi}{2\Omega_x}} \left(\frac{\text{Da}}{\pi} \right)^{1/4} t^{-1/4} \quad (\text{B8})$$

which is independent of the value of α , and scales like $t^{-1/4}$. These results are in agreement with the observations in the particle tracking simulations. In figure 8 we plot the evolution of the average concentration over time by solving equations (31) and (32) numerically, using the finite domain Green's function in (B3), instead of its infinite domain counterpart.

The results in the figure are very similar to those observed in the numerical simulations, particularly in that at late times all solutions for $\alpha \neq 0$ collapse on to the same curve. This scaling can also be interpreted physically as a boundary effect as follows. At the relevant late times, the single-reactant islands span the full width of the domain and the system essentially becomes one dimensional. The late time incomplete-mixing scaling is known to behave as $t^{-d/4}$, which matches our findings [18]. This again demonstrates the utility of the simple proposed closure in interpreting the results observed in the numerical simulations. As a cautionary note, we would again like to highlight that the proposed closure is not exact; the good agreement with simulations is promising, but further work is required to refine it rigorously.

ACKNOWLEDGMENTS

P.A. would like to acknowledge partial funding by the Startup grant of the V.P. of research in TAU. T.A. gratefully acknowledges support by the Portuguese Foundation for Science and Technology (FCT) under Grant SFRH/BD/89488/2012. D.B. would like to acknowledge partial funding via NSF grant EAR-1351625 and EAR-1417264 as well as the U. S. Army Research Laboratory and the U. S. Army Research Office under contract/grant number W911NF1310082. The authors thank the two anonymous reviewers for their con-

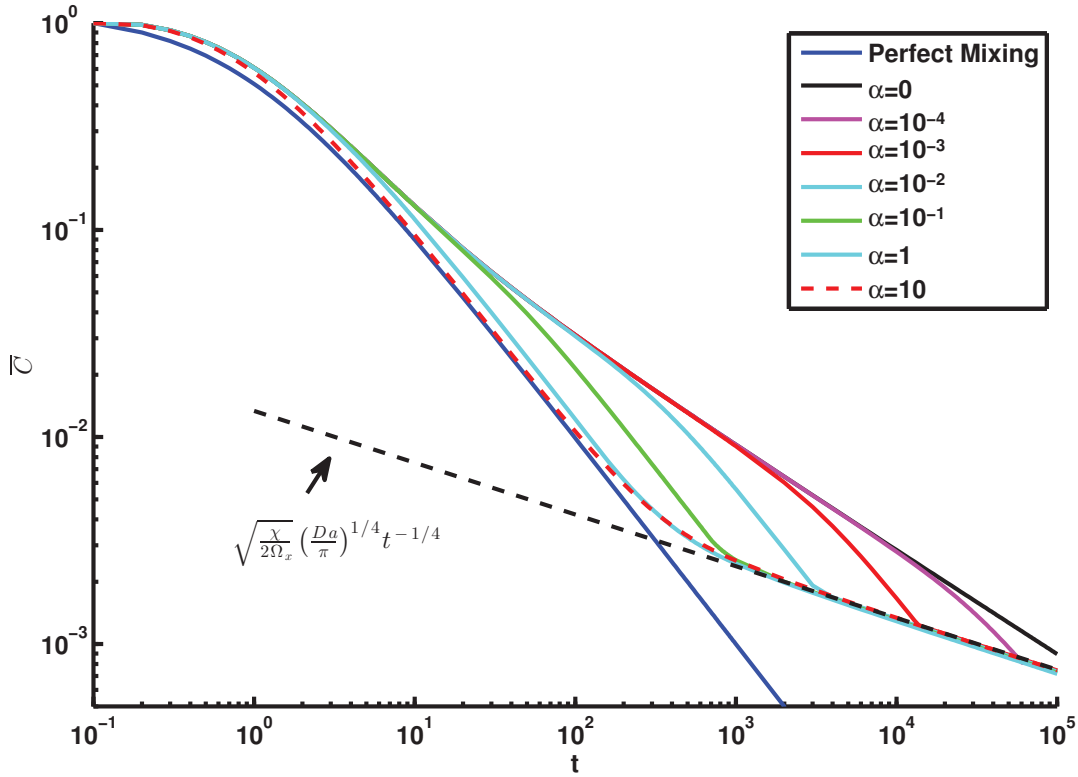


FIG. 8. (Color online) Numerical solution for the average concentration using the finite domain Green's function in equation (B1) for various α , $Da = 10$ and $\chi = 0.01$. In this figure α is varied to show how it affects the transition between each of the scaling regimes. Note the collapse of all late time scalings on to the same line $\bar{C}_i(t) = \sqrt{\frac{\chi}{2\Omega_x}} \left(\frac{Da}{\pi}\right)^{1/4} t^{-1/4}$, in agreement with observations from numerical simulations.

structive comments on the manuscript.

-
- [1] J. Seinfeld and S. Pandis, *Atmospheric Chemistry and Physics: From Air Pollution to Climate Change* (Wiley, 2006).
 - [2] I. Mezić, S. Loire, V. Fonoberov, and P. Hogan, *Science* **330**, 486 (2010).
 - [3] C. Escauriaza, C. Gonzalez, P. Guerra, P. Pasten, and G. Pizarro, *Bulletin of the American Physical Society* **57** (2012).
 - [4] P. Znachor, V. Visocká, J. Nedoma, and P. Rychtecký, *Freshwater Biology* (2013).
 - [5] J. Sierra-Pallares, D. Marchisio, E. Alonso, M. Teresa Parra-Santos, F. Castro, and

- M. José Cocero, Chemical engineering science (2011).
- [6] W. Stockwell, Meteorology and Atmospheric Physics **57**, 159 (1995).
- [7] L. Whalley, K. Furneaux, A. Goddard, J. Lee, A. Mahajan, H. Oetjen, K. Read, N. Kaaden, L. Carpenter, A. Lewis, *et al.*, Atmospheric Chemistry and Physics **10**, 1555 (2010).
- [8] T. Michioka and S. Komori, AIChE journal **50**, 2705 (2004).
- [9] J. Pauer, K. Taunt, W. Melendez, R. Kreis Jr, and A. Anstead, Journal of Great Lakes Research **33**, 554 (2007).
- [10] C. Gramling, C. Harvey, and L. Meigs, Environ Sci Technol. **36**, 2508 (2002).
- [11] M. de Simoni, J. Carrera, X. Sanchez-Vila, and A. Guadagnini, Water Resources Research **41**, W11410 (2005).
- [12] P. d. Anna, J. Jimenez-Martinez, H. Tabuteau, R. Turuban, T. Le Borgne, M. Derrien, and Y. Mheust, Environmental science & technology **48**, 508 (2013).
- [13] P. De Anna, M. Dentz, A. Tartakovsky, and T. Le Borgne, Geophysical Research Letters **41**, 4586 (2014).
- [14] M. Dentz and J. Carrera, Physics of Fluids (1994-present) **19**, 017107 (2007).
- [15] D. Gillespie, Journal of Chemical Physics **113**, 297 (2000).
- [16] A. Ovchinnikov and Y. Zeldovich, Chem. Phys. **28**, 215 (1978).
- [17] D. Toussaint and F. Wilczek, J. Chem. Phys. **78**, 2642 (1983).
- [18] K. Kang and S. Redner, Physical Review Letters **52**, 955 (1984).
- [19] E. Monson and R. Kopelman, Physical review letters **85**, 666 (2000).
- [20] E. Monson and R. Kopelman, Physical Review E **69**, 021103 (2004).
- [21] A. M. Tartakovsky, P. de Anna, T. Le Borgne, A. Balter, and D. Bolster, Water Resources Research **48**, W02526 (2012).
- [22] G. Zumofen, J. Klafter, and M. Schlesinger, Physical Review Letters **77**, 2830 (1996).
- [23] D. Bolster, P. de Anna, D. A. Benson, and A. M. Tartakovsky, Advances in Water Resources **37**, 86 (2012).
- [24] R. Klages and I. Radons, Gand Sokolov, *Anomalous transport: foundations and applications* (John Wiley & Sons, 2008).
- [25] D. Koch and J. Brady, Journal of Fluid Mechanics **180**, 387 (1987).
- [26] D. Koch and J. Brady, Physics of Fluids (1958-1988) **31**, 965 (1988).
- [27] D. Koch, R. Cox, H. Brenner, and J. Brady, Journal of Fluid Mechanics **200**, 173 (1989).

- [28] F. Boano, A. Packman, A. Cortis, R. Revelli, and L. Ridolfi, Water resources research **43** (2007).
- [29] B. Berkowitz, A. Cortis, M. Dentz, and H. Scher, Reviews of Geophysics **44** (2006).
- [30] D. Benson and S. Wheatcraft, Transport in Porous Media **42**, 211 (2001).
- [31] F. Höfling and T. Franosch, Reports on Progress in Physics **76**, 046602 (2013).
- [32] S. Jones and W. Young, Journal of Fluid Mechanics **280**, 149 (1994).
- [33] C. Escauriaza and F. Sotiropoulos, Journal of Fluid Mechanics **641**, 169 (2009).
- [34] H. Aref and S. Balachandar, Physics of Fluids (1958-1988) **29**, 3515 (1986).
- [35] T. Solomon and J. Gollub, Physical Review A **38**, 6280 (1988).
- [36] Z. Pouransari, M. Speetjens, and H. Clercx, Journal of Fluid Mechanics **654**, 5 (2010).
- [37] M. Latini and A. Bernoff, Journal of Fluid Mechanics **441**, 399 (2001).
- [38] P. Shankar, Journal of Fluid Mechanics **631**, 363 (2009).
- [39] A. Okubo, J. Oceanogr. Soc. Japan **24**, 20 (1968).
- [40] A. Okubo and M. J. Karweit, Limnology and Oceanography , 514 (1969).
- [41] E. Novikov, Journal of Applied Mathematics and Mechanics **22**, 576 (1958).
- [42] G. Csanady, *Turbulent Diffusion in the Environmnet*, Geophysics and Astrophysics Monographs, Vol. 3 (D. Reidel publishing company, 1973) pp. 147–148.
- [43] H. Tennekes and J. L. Lumley, *A first course in turbulence* (MIT press, 1972).
- [44] A. Monin and A. Yaglom, *Statistical fluid mechanics: mechanics of turbulence*, Vol. 1 (Courier Dover Publications, 2007).
- [45] D. Bolster, M. Dentz, and T. Le Borgne, Water Resources Research **47**, W09602 (2011).
- [46] S. Pope, *Turbulent flows* (Cambridge university press, 2000).
- [47] T. LeBorgne, M. Dentz, D. Bolster, J. Carrera, J. deDreuzy, and P. Davy, Advances in Water Resources **33**, 1468 (2010).
- [48] P. Kitanidis, Water Resources Research **30**, 2011 (1994).
- [49] F. de Barros, M. Dentz, J. Koch, and W. Nowak, Geophysical Research Letters **39**, L08404 (2012).
- [50] D. A. Benson and M. M. Meerschaert, Water Resources Research **44**, W12201 (2008).
- [51] A. Paster, D. Bolster, and D. A. Benson, Journal of Computational Physics **263**, 91 (2014).
- [52] D. Bolster, M. Dentz, and J. Carrera, Water resources research **45** (2009).
- [53] A. Paster, D. Bolster, and D. A. Benson, Water Resources Research **49**, 1 (2013).

- 712 [54] G. Dagan, *Flow and Transport in Porous Formations*, 804 (Springer-Verlag, New-York, 1989).
- 713 [55] K. Candan and M. Sapino, *Data Management for Multimedia Retrieval* (Cambridge University
714 Press, 2010).
- 715 [56] H. Risken, *Fokker-Planck Equation* (Springer, 1984).
- 716 [57] D. Dentz, D. Bolster, N. Engdahl, and T. Aquino, *Advances in Water Resources* **Submitted**
717 (2014).
- 718 [58] A. Tartakovsky, P. Anna, T. Le Borgne, A. Balter, and D. Bolster, *Water Resources Research*
719 **48** (2012).
- 720 [59] A. Paster and D. Bolster, *Physica A: Statistical Mechanics and its Applications* **391**, 4654
721 (2012).